Spectrometric reconstruction of mechanical-motional states in optomechanics

Jie-Qiao Liao[1] and Franco Nori[1,2]

[1]*CEMS, RIKEN, Saitama 351-0198, Japan*
[2]*Department of Physics, The University of Michigan, Ann Arbor, Michigan 48109-1040, USA*

We propose a spectrometric method to reconstruct the motional states of mechanical modes in optomechanics. This is achieved by detecting the single-photon emission and scattering spectra of the optomechanical cavity. Owing to an optomechanical coupling, the *a priori* phonon-state distributions contribute to the spectral magnitude, and hence we can infer information on the phonon states from the measured spectral data. When the single-photon optomechanical-coupling strength is moderately larger than the mechanical frequency, then our method works well for a wide range of cavity-field decay rates, irrespective of whether or not the system is in the resolved-sideband regime.

I. INTRODUCTION

Quantum states carry complete information of a physical system. To obtain the statistical properties of the system, one needs to know its state vector or density operator when it is in a pure or mixed state, respectively [1]. Quantum-state tomography (QST) is a procedure for reconstructing the state of quantum systems by measuring a complete set of observables [2–4]. In the past two decades, many advances have been made in QST for both continuous-variable [4] and discrete-variable [5–7] states. For example, the QST of a harmonic oscillator has been analyzed in both quadrature and Fock-state representations. Moreover, quantum-state reconstruction has also been studied on optical [8–12] and microwave [13–19] photon fields, as well as the motional states of matter systems, such as atoms [20–22], molecules [23,24], and micro- or nanomechanical resonators [25–27].

Generally, it is a difficult task to directly reconstruct the quantum state of a massive mechanical resonator because one cannot access the mechanical excitation directly. Usually, other auxiliary systems, such as optical modes [28,29] or atoms [26] are needed to transduce the states of mechanical modes. In this sense, optomechanical systems [30,31] can provide a natural platform to perform this task because there is an inherent interface between mechanical and optical modes. Even though people have noticed the means for controlling mechanical motion (e.g., cooling [32–35] and quantum-state engineering [36–43]) by designing proper driving fields, the method for monitoring the mechanical motion in the nonlinear quantum optomechanics via the optical means remains mostly unexplored. We note that QST in optomechanics has recently been studied in the short-pulse case [28,29] and in optically-levitating-dielectrics systems [44].

In this paper, we propose a reliable method for reconstructing the mechanical motional state of the moving mirror in cavity optomechanics. Our approach is based on spectrometric measurement of the emission or scattering of a single photon interacting with the mechanical motion. Owing to the optomechanical coupling, the mechanical oscillation will modulate the behavior of the single photon (which will show in its spectrum), and hence one can infer the state information of the mechanical mode from the measured spectral data.

II. THE SYSTEM

We start by considering an open optomechanical cavity, which is formed by a fixed end mirror and a moving end mirror, as shown in Fig. 1. Assuming that the moving mirror is perfect and the fixed mirror is partially transparent, then the cavity fields couple with the continuous fields outside the cavity through photon-hopping interactions. In a rotating frame with respect to $H_0 = \omega_c a^\dagger a + \omega_c \int_0^\infty c_k^\dagger c_k dk$ ($\hbar = 1$), the Hamiltonian of the total system including the cavity and the environment fields is [45,46]

$$H_s = H_{\text{opc}} + \int_0^\infty \Delta_k c_k^\dagger c_k dk + \int_0^\infty \xi_k(a^\dagger c_k + c_k^\dagger a)dk, \quad (1)$$

with $H_{\text{opc}} = \omega_M b^\dagger b - g_0 a^\dagger a(b^\dagger + b)$. Here, $a(a^\dagger)$ and $b(b^\dagger)$ are, respectively, the annihilation (creation) operators of the optical and mechanical modes, with respective frequencies ω_c and ω_M. The second term in H_{opc} describes the radiation-pressure coupling, and g_0 is the single-photon optomechanical coupling strength [47]. The annihilation and creation operators c_k and $c_k^\dagger$ describe the kth mode of the outside fields with resonant frequency ω_k. The parameter $\Delta_k = \omega_k - \omega_c$ is the detuning between the frequencies of the kth mode and the cavity mode. The coupling between the cavity field and the outside fields is described by the photon-hopping interaction with coupling strength ξ_k. Under the framework of the Wigner–Weisskopf theory, the parameter ξ_k is related to the photon decay rate by $\gamma_c = 2\pi\xi_c^2$, where ξ_c is the strength at the cavity resonance frequency. We note that the Hamiltonian of the total system in the Schrödinger picture can be written as $H = H_0 + H_s$ because of $[H_0, H_s] = 0$.

Because the mechanical decay rate γ_M is much smaller than the optical decay rate γ_c ($\gamma_M/\gamma_c \sim 10^{-3}$ to 10^{-7} in typical optomechanical systems [31]), in this paper we will merely take the photon decay into account and neglect the mechanical dissipation. This treatment is justified because the photon emission and scattering processes are completed in a time scale $1/\gamma_c$ during which the mechanical dissipation is negligible.

III. SINGLE-PHOTON SPECTRA

In this system, the total photon-number operator $T_p = a^\dagger a + \int_0^\infty c_k^\dagger c_k dk$ is a conserved quantity, due to $[T_p, H] = 0$,
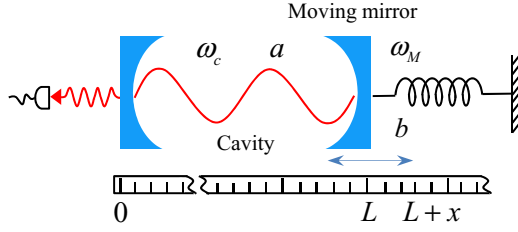
FIG. 1. (Color online) Schematic diagram of a Fabry–Perot-type optomechanical cavity formed by a fixed end mirror and a moving end mirror. The cavity fields couple with the continuous fields outside the cavity through photon-hopping interactions.

then we can restrict the system within a subspace with a definite photon number. In the single-photon subspace, a general pure state of the total system can be written as

$$|\varphi(t)\rangle = \sum_{l=0}^{\infty} A_l(t)|1\rangle_a |\tilde{l}\rangle_b |\emptyset\rangle$$
$$+ \sum_{l=0}^{\infty} \int_0^{\infty} B_{l,k}(t)|0\rangle_a |l\rangle_b |1_k\rangle dk, \qquad (2)$$

where $|\tilde{l}\rangle_b = \exp[\beta_0(b^\dagger - b)]|l\rangle_b$ are single-photon-displaced phonon-number states [48] with $\beta_0 = g_0/\omega_M$. The states $|\tilde{l}\rangle_b$ are defined by the eigenequation

$$[\omega_M b^\dagger b - g_0(b^\dagger + b)]|\tilde{l}\rangle_b = (l\omega_M - \delta)|\tilde{l}\rangle_b, \qquad (3)$$

with $\delta = g_0^2/\omega_M$. Here the Hamiltonian operator at the left-hand side of Eq. (3) is H_{opc} when the photon number is limited to one. In Eq. (2), $|1_k\rangle = c_k^\dagger|\emptyset\rangle$ is the single-photon state of mode c_k, and $|\emptyset\rangle$ is the vacuum state. The first and second components in $|\varphi(t)\rangle$ denote the basis states for the single photon in the cavity mode and the kth mode outside the cavity, respectively. The variables $A_l(t)$ and $B_{l,k}(t)$ are probability amplitudes.

In the long-time limit $t \gg 1/\gamma_c$, the single photon completely leaks out of the cavity, regardless of its initial state, then $A_l(\infty) = 0$ and the long-time state becomes

$$|\varphi(\infty)\rangle = \sum_{l=0}^{\infty} \int_0^{\infty} B_{l,k}(\infty)|0\rangle_a |l\rangle_b |1_k\rangle dk. \qquad (4)$$

The form of $B_{l,k}(\infty)$ depends on the initial state of the system. Here, the single photon could be initially in either the cavity or the outside fields. These two cases correspond to the single-photon emission and scattering processes.

Below, we derive the single-photon emission and scattering spectra when the mechanical resonator is in an arbitrary initial state. This is achieved by first calculating the spectra corresponding to the mirror initially in a Fock state $|n_0\rangle_b$, and then we obtain the spectra for a general initial state by superposition. When the mirror is initially in the number state $|n_0\rangle_b$, the initial state of the total system is

$$|\varphi_{n_0}(0)\rangle = |n_0\rangle_b |\phi\rangle_{\text{photon}}. \qquad (5)$$

In the single-photon-emission case, the single photon is initially in the cavity, and we have $|\phi\rangle_{\text{photon}} = |1\rangle_a |\emptyset\rangle$. In the scattering case, the cavity is initially in a vacuum and the single

photon is in a Lorentzian wave packet in the continuous fields. Then the initial state of the photon is

$$|\phi\rangle_{\text{photon}} = |0\rangle_a \otimes \sqrt{\frac{\epsilon}{\pi}} \int_0^{\infty} \frac{1}{(\Delta_k - \Delta_0 + i\epsilon)}|1_k\rangle dk, \qquad (6)$$

where Δ_0 and ϵ are the wave-packet center and width, respectively. At time t, the state of the system can be expressed as Eq. (2), with the replacements $|\varphi(\infty)\rangle \to |\varphi_{n_0}(\infty)\rangle$, $A_l(t) \to A_{n_0,l}(t)$, and $B_{l,k}(t) \to B_{n_0,l,k}(t)$. Here the subscript n_0 in state $|\varphi_{n_0}(t)\rangle$ and probability amplitudes $A_{n_0,l}(t)$ and $B_{n_0,l,k}(t)$ refers to the initial state $|n_0\rangle_b$ of the mirror. The expressions of $A_{n_0,l}(t)$ and $B_{n_0,l,k}(t)$ for the single-photon-emission and -scattering cases have been given in Ref. [45]. In the single-photon-emission and -scattering cases, we can check that the state of the system is normalized, i.e., $\langle\varphi_{n_0}(t)|\varphi_{n_0}(t)\rangle = 1$. Since we treat the optomechanical system and the continuous fields outside the cavity as a whole closed system, the evolution of the total system is unitary. We should point out that, in the derivation of the analytical expression of these probability amplitudes, we have made the Wigner–Weisskopf approximation.

Based on the above discussions, we denote the relation

$$|\varphi_{n_0}(t)\rangle = U(t)|\varphi_{n_0}(0)\rangle = U(t)|n_0\rangle_b |\phi\rangle_{\text{photon}}, \qquad (7)$$

where $U(t)$ is the unitary evolution operator associated with the Hamiltonian H_s of the total system. Therefore, when the mirror is initially in a general density matrix

$$\rho^{(b)}(0) = \sum_{m,n=0}^{\infty} \rho_{m,n}^{(b)}(0)|m\rangle_b\,_b\langle n|, \qquad (8)$$

with $\rho_{m,n}^{(b)}(0) = \,_b\langle m|\rho^{(b)}(0)|n\rangle_b$, the state of the total system at time t would be

$$\rho(t) = U(t)[\rho^{(b)}(0) \otimes |\phi\rangle_{\text{photon photon}}\langle\phi|]U^\dagger(t)$$
$$= \sum_{m,n=0}^{\infty} \rho_{m,n}^{(b)}(0)U(t)|m\rangle_b |\phi\rangle_{\text{photon photon}}\langle\phi|\,_b\langle n|U^\dagger(t)$$
$$= \sum_{m,n=0}^{\infty} \rho_{m,n}^{(b)}(0)|\varphi_m(t)\rangle\langle\varphi_n(t)|. \qquad (9)$$

Correspondingly, the long-time state of the total system is

$$\rho(\infty) = \sum_{m,n=0}^{\infty} \rho_{m,n}^{(b)}(0)|\varphi_m(\infty)\rangle\langle\varphi_n(\infty)|, \qquad (10)$$

where $|\varphi_{m(n)}(\infty)\rangle = \sum_{l=0}^{\infty} \int_0^{\infty} B_{m(n),l,k}(\infty)|0\rangle_a |l\rangle_b |1_k\rangle dk$. From $\rho(\infty)$ we obtain the single-photon spectra

$$S(\Delta_k) \equiv \text{Tr}[\Pi_k \rho(\infty)] = \sum_{m,n=0}^{\infty} \rho_{m,n}^{(b)}(0)\Lambda_{n,m}(\Delta_k), \qquad (11)$$

where $\Pi_k = |1_k\rangle\langle 1_k|$ is the single-photon projective operator and

$$\Lambda_{n,m}(\Delta_k) = \sum_{l=0}^{\infty} B_{n,l,k}^*(\infty)B_{m,l,k}(\infty). \qquad (12)$$

The relation (11) is important in this work and provides the connection between the spectra and the density-matrix

elements of the mirror. This result motivates us to reconstruct the initial state of the mirror by measuring the spectra of the outgoing photon.

IV. QUANTUM-STATE RECONSTRUCTION

A. Diagonal density-matrix case

To better see this procedure, we first consider the diagonal density-matrix case, where the density matrix is diagonal in the basis of number states. In this case, the initial state of the mirror is assumed to be $\rho^{(b)}(0) = \sum_{n=0}^{\infty} P_n |n\rangle_{b\,b}\langle n|$, with the phonon-number distribution P_n. Then, the single-photon spectra become $S(\Delta_k) = \sum_{n=0}^{\infty} P_n S_{|n\rangle_b}(\Delta_k)$, where $S_{|n\rangle_b}(\Delta_k) = \Lambda_{n,n}(\Delta_k)$ are the spectra corresponding to the component of the Fock state $|n\rangle_b$. Once we know the three parameters g_0, γ_c, and ω_M, then $S_{|n\rangle_b}(\Delta_k)$ can be obtained. In realistic reconstructions, we approximately truncate the Hilbert space of the mirror into the lowest N-dimensional subspace. Here the dimension parameter N should be chosen to be sufficiently large such that the probabilities outside this subspace are negligible. In this case, the spectra can be approximated by

$$S(\Delta_k) \approx \sum_{n=0}^{N-1} P_n S_{|n\rangle_b}(\Delta_k). \tag{13}$$

Inspired by this relation, we construct a system of linear equations for the variables P_n by choosing N sample points (with the coordinates Δ_{k_j}, $j = 1, 2, 3, \ldots, N$) from the spectra. The compact form of these equations is

$$\mathbf{KP} = \mathbf{Q}, \tag{14}$$

where $\mathbf{P} = (P_0, P_1, \ldots, P_{N-1})^T$. The elements of $\mathbf{K}$ and $\mathbf{Q}$ are defined by

$$K_{j,j'} = S_{|j'-1\rangle_b}(\Delta_{k_j}), \quad Q_j = S(\Delta_{k_j}), \tag{15}$$

for $j, j' = 1, 2, 3, \ldots, N$. The square matrix $\mathbf{K}$ can be calculated based on the parameters g_0, γ_c, and ω_M, and the vector $\mathbf{Q}$ can be measured in experiments. Therefore, if the square matrix $\mathbf{K}$ is full rank, then the phonon-number distribution can be obtained as

$$\mathbf{P} = \mathbf{K}^{-1}\mathbf{Q}, \tag{16}$$

where $\mathbf{K}^{-1}$ is the inverse matrix of $\mathbf{K}$ (see the appendix for an example).

One crucial factor in our method is to keep the validity of the truncation approximation in Eq. (13); namely, we need to choose a proper truncation dimension N. A natural question arises: for a unknown initial state of the mirror, how to choose a proper N? In a realistic simulation, we need to choose tentative values of N many times by increasing N step by step. For an insufficiently large N, the reconstructed elements are incorrect and hence do not converge. We keep on increasing N step by step until the reconstructed data converge. Then this value of N will be good enough to satisfy Eq. (13). If the N used is larger than the dimension of the exact space; namely, the number of nonzero probabilities, then the additional phonon probabilities will be zero in the solution. In this case, $\mathbf{K}$ is still a square matrix.
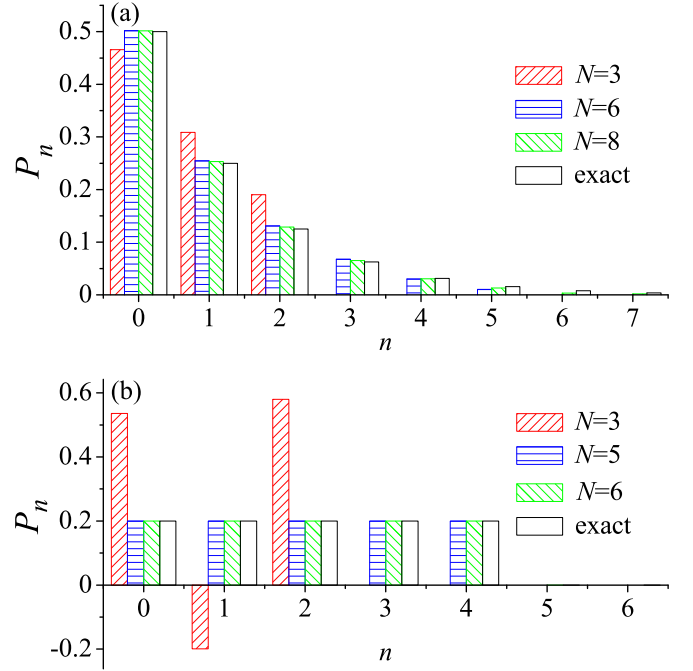

FIG. 2. (Color online) Reconstructed phonon-number distributions P_n, based on the emission spectrum, for various values of the dimension parameter N; the exact distribution is presented for reference. Here the initial state of the mirror is (a) the thermal state $\rho_{\rm th}^{(b)} = \sum_{n=0}^{\infty} [\bar{n}_{\rm th}^n/(\bar{n}_{\rm th}+1)^{n+1}]|n\rangle_{b\,b}\langle n|$, with $\bar{n}_{\rm th} = 1$, (b) the maximally mixed state $\rho_{\rm mms}^{(b)} = \frac{1}{\sqrt{n_s}}\sum_{l=0}^{n_s-1}|l\rangle_{b\,b}\langle l|$ in a subspace of dimension $n_s = 5$. Other parameters are $\gamma_c/\omega_M = 0.1$ and $g_0/\omega_M = 2$.

As examples, below we demonstrate our method by considering two typical mixed states: the thermal state

$$\rho_{\rm th}^{(b)} = \sum_{n=0}^{\infty} \frac{\bar{n}_{\rm th}^n}{(\bar{n}_{\rm th}+1)^{n+1}} |n\rangle_{b\,b}\langle n|, \tag{17}$$

and the maximally mixed state

$$\rho_{\rm mms}^{(b)} = \frac{1}{n_s} \sum_{n=0}^{n_s-1} |n\rangle_{b\,b}\langle n| \tag{18}$$

in a subspace of dimension n_s (with $P_n = 1/n_s$ for $n = 0, 1, 2, \ldots, n_s - 1$, and $P_n = 0$ for others). The reconstructed phonon distributions are shown in Fig. 2, which are compared with the exact phonon distributions. It can be seen from Fig. 2(a) that the reconstructed distributions become more stable and eventually converge with increasing N. The stable data correspond to a good truncation approximation in Eq. (13). The fidelities between the reconstructed and exact phonon-number distributions are $F = 0.841, 0.980, 0.993$ for $N = 3, 6, 8$ in Fig. 2(a). This truncation effect is more obvious for the state $\rho_{\rm mms}^{(b)}$. As shown in Fig. 2(b), the reconstructed distributions become stable as long as $N \geqslant n_s$. For this state, when $N \geqslant n_s$, the relation (13) is exact because the Hilbert space is truncated automatically.

Equation (13) indicates that, once the dimension parameter N is large enough to satisfy the truncation approximation, the reconstructed distributions should be independent of the

choice of the sample points. Nevertheless, we should choose the sample points such that the vector **Q** can capture the spectral feature as much as possible; mathematically, making sure the matrix **K** is full rank. In Fig. 2, the sample points are located at

$$\Delta_{k_j} = -\delta + j\omega_M, \quad j = \lfloor -N/2, \ldots, N/2 \rfloor, \quad (19)$$

where $\delta = g_0^2/\omega_M$. These locations correspond to the phonon sideband peaks and can hence mostly capture the spectral feature. In Fig. 3(a), we reconstruct the phonon distributions using three groups of random sample points in the region $\Delta_{k_j}/\omega_M \in [-5,5]$. The results show that the reconstructed results are well consistent with the exact results (with fidelities $F > 0.994$), and that our approach is almost independent of the choice of sample points.

Two inherent dimensionless parameters in this system are the scaled single-photon optomechanical coupling strength g_0/ω_M and the scaled cavity-field decay rate γ_c/ω_M [49–52]. In order to see how our approach depends on these parameters, we show the reconstructed phonon distributions for various values of the two ratios. As shown in Fig. 3(b), we can see that our approach works well for a moderately large coupling strength. Our numerical results show that the optomechanical-coupling strength should be on the scale of $g_0/\omega_M \sim 2$. A too-weak optomechanical coupling cannot capture the information regarding the phonon distribution from the spectra and cannot make sure **M** becomes full rank. On the contrary, a large g_0 will increase the computational difficulties because the involved Hilbert space for phonons is large. In addition, for the cavity-field decay rate γ_c, there is a wide range to choose. Figure 3(c) proves that our approach works well over a wide parameter range, irrespective of whether the system is in the resolved-sideband regime.

Our method can also be realized based on the scattering spectrum. In the scattering case, in addition to the parameters g_0, γ_c, and ω_M, there are two additional controllable parameters: the wave-packet center Δ_0 and the width ϵ of the incident photon. In Fig. 3(d), we plot the reconstructed phonon distributions for various parameters based on the scattering spectrum. We can see that our method works well in both the narrow-wave-packet ($\epsilon/\omega_M \ll 1$) and wide-wave-packet ($\epsilon/\omega_M > 1$) cases. In addition, it also works well for a wide range of driving frequencies, which correspond to different phonon sideband resonant transitions [45].

B. General density-matrix case

We now consider the general density-matrix case, in which the density matrix contains nonzero off-diagonal elements in the number-state representation. By truncating the Hilbert space, the single-photon spectra in Eq. (11) can be approximated by

$$S(\Delta_k) \approx \sum_{m,n=0}^{N-1} \rho_{m,n}^{(b)}(0)\Lambda_{n,m}(\Delta_k). \quad (20)$$

By choosing N^2 sample points (with locations Δ_{k_j}, $j = 1,2,3,\ldots,N^2$) in the spectra, we can construct a system of
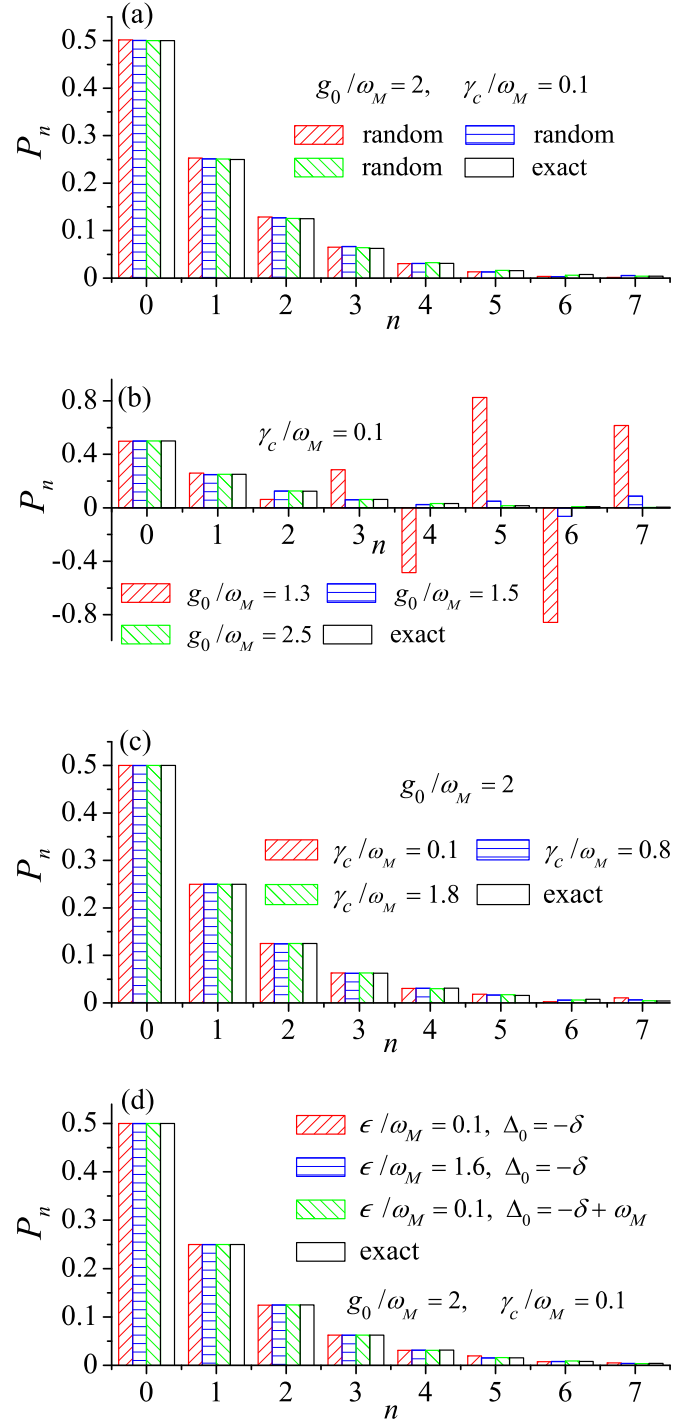

FIG. 3. (Color online) Reconstructed thermal phonon-number distributions P_n based on (a)–(c) emission and (d) scattering spectra in various cases. (a) The sample points are chosen randomly in the region $\Delta_{k_j}/\omega_M \in [-5,5]$. The reconstructed distributions for various values of (b) the single-photon optomechanical coupling strength g_0 or of (c) the cavity-field decay rate γ_c. (d) The distributions are reconstructed based on the scattering spectrum for various values of the parameters ϵ and Δ_0. Here we choose $\bar{n}_{th} = 1$, and other parameters are shown in the panels.

linear equations of these density-matrix elements as

$$\mathbf{MC} = \mathbf{R}, \quad (21)$$

where the coefficient matrix $\mathbf{M}$ and the column vector $\mathbf{R}$ are defined by

$$\mathbf{M}_{j,j'} = \Lambda_{n,m}(\Delta_{k_j}), \quad \mathbf{R}_j = S(\Delta_{k_j}), \quad (22)$$

for $j, j' = 1, 2, 3, \ldots, N^2$. The relationship between the variables m, n and j' is

$$m = \text{Floor}[(j'-1)/N], \quad n = (j'-1) - mN, \quad (23)$$

where the function $\text{Floor}(x)$ gives the greatest integers less than or equal to x. The vector $\mathbf{C}$ is the variable to be determined, its elements

$$\mathbf{C}_l = \rho_{m,n}^{(b)}(0), \quad l = 1, 2, 3, \ldots, N^2, \quad (24)$$

are the density-matrix elements for the initial state of the moving mirror, where the relationship between the variables m, n, and l is $m = \text{Floor}[(l-1)/N]$ and $n = (l-1) - mN$.

If the square matrix $\mathbf{M}$ is full rank, then the unique solution of these density-matrix elements can be obtained as

$$\mathbf{C} = \mathbf{M}^{-1}\mathbf{R}, \quad (25)$$

where $\mathbf{M}^{-1}$ is the inverse matrix of $\mathbf{M}$. The vector $\mathbf{R}$ can be obtained by experimentally detecting the single-photon spectra, and the coefficient matrix $\mathbf{M}$ can be determined from the expression of $\Lambda_{n,m}(\Delta_k)$ for special values $\Delta_k = \Delta_{k_j}$; then we can reconstruct the initial density matrix of the mechanical mode (see the appendix for an example). As additional examples, we consider the density-matrix reconstruction for Fock states and superposed Fock states based on the emission spectrum. The reconstructed density-matrix elements are shown in Fig. 4 for states $|0\rangle_b$, $|1\rangle_b$, $|2\rangle_b$, $(|0\rangle_b \pm |1\rangle_b)/\sqrt{2}$, and $(|0\rangle_b + |1\rangle_b + |2\rangle_b)/\sqrt{3}$. The data obtained is consistent with the exact result with high fidelities $F > 0.999$.

V. DISCUSSIONS AND CONCLUSIONS

There are two important factors in the experimental implementation of our method: (i) The single-photon optomechanical coupling strength g_0 should be moderately larger than the resonant frequency ω_M of the mechanical resonator, i.e., $g_0/\omega_M \sim 2$. An optomechanical coupling at this scale can be realized in ultracold atoms. In Ref. [50], a coupling of $g_0/\omega_M > 10$ has been realized. In particular, our method does not require the resolved-sideband condition $g_0 > \gamma_c$, making this proposal experimentally feasible. However, in most optomechanical systems [31], the optomechanical coupling strengths are much smaller than the mechanical frequencies. Recently, two theoretical proposals have been proposed to enhance the optomechanical couplings (the estimated g_0 is several MHz) in electromechanics [53,54]. Moreover, the ratio g_0/ω_M can also be increased by introducing either modulated optomechanical couplings [55], mechanical normal modes [56], or collective mechanical modes in a transmissive scatter array [57]. (ii) How to measure the single-photon emission and scattering spectra is a key step for the realization of this method. In experiments, to profile the pattern of single-photon spectra, the single photon needs to be detected by sweeping the frequency [58].

We note that there is no postselection in our method. This is because we do not need to condition a probability space. In our system, the total photon number is a conserved quantity,
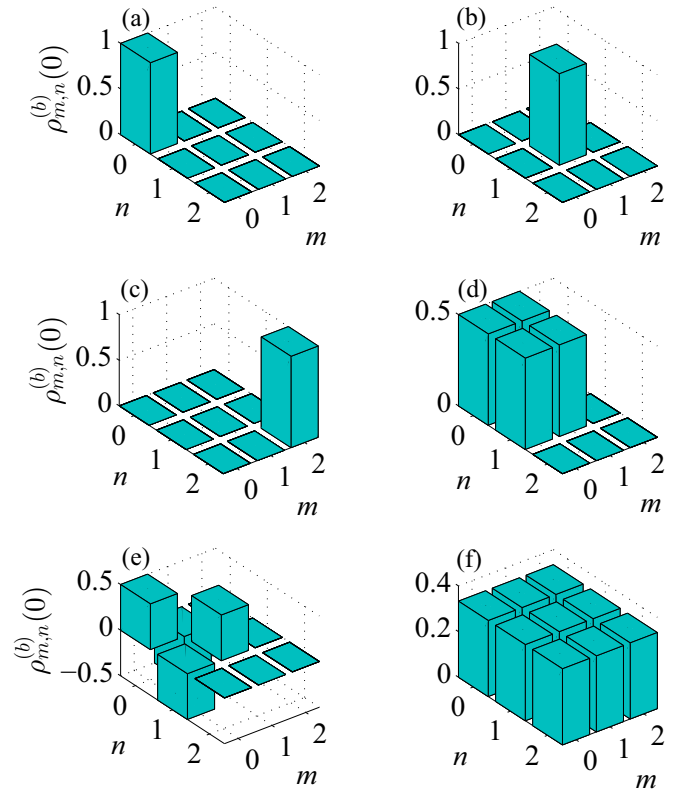

FIG. 4. (Color online) Reconstructed density-matrix elements $\rho_{m,n}^{(b)}(0)$ based on the emission spectrum for various states: (a)–(c) Fock states $|0\rangle_b$, $|1\rangle_b$, and $|2\rangle_b$, (d), (e) superposed Fock states $(|0\rangle_b \pm |1\rangle_b)/\sqrt{2}$, and (f) $(|0\rangle_b + |1\rangle_b + |2\rangle_b)/\sqrt{3}$. Other parameters are $\gamma_c/\omega_M = 0.1$ and $g_0/\omega_M = 2$.

and hence we can restrict the system within the single-photon subspace. Namely, a single photon is initially prepared in the cavity (emission) or the continuous field outside the cavity (scattering), after the interaction with the mechanical motion, the single photon will leak out of the cavity due to the photon decay channel. Finally, we measure the spectrum of the single photon, i.e., the reservoir photon occupation distribution. During these processes, there is one and only one photon. Hence, the states of the mechanical motions are completely obtained by measuring the spectrum of the single photon, without postselection.

To conclude, we have proposed a spectrometric approach for reconstructing the mechanical motional state in optomechanics by detecting single-photon spectra. We considered two different situations: single-photon emission and scattering, which correspond to the cases where the single photon is initially in the cavity field or in a wave packet in the continuous fields outside the cavity. In our considerations, the mechanical dissipation was safely neglected, because the mechanical dissipation is negligible during the time interval for the single-photon emission and scattering to be finished. However, our studies included the photon dissipation by modeling the optical environment as a harmonic-oscillator bath, under the framework of the Wigner–Weisskopf approximation. Our method has a mild constraint in the cavity-field decay rate: it works well in both the sideband-resolved and unresolved regimes. However, the single-photon

coupling strength g_0 should satisfy $g_0/\omega_M \sim 2$, such that the single-photon spectra can capture the phonon-state information. In the single-photon strong-coupling regime, the non-Gaussian effects are observable. Much recent attention has been paid to explore the non-Gaussian physics in this parameter regime. Nevertheless, quantum-state tomography in this regime remains mostly unexplored and here we have proposed a method for tomography in this regime. Moreover, our method is general and can be potentially realized in various optomechanical systems [31]. And the idea of spectrometric reconstruction of quantum states can be applied to quadratic optomechanics [59] and cavity QED [60].

ACKNOWLEDGMENTS

APPENDIX: EXAMPLES FOR QUANTUM-STATE RECONSTRUCTION BASED ON SINGLE-PHOTON-EMISSION SPECTRUM

In this Appendix, we present two examples to show how to simulate quantum-state reconstruction of a diagonal or a general density matrix in the number-state representation, based on the single-photon emission spectrum.

1. Single-photon-emission solution

In the single-photon-emission case, the probability amplitude $B_{n_0,l,k}(\infty)$ has been given in Ref. [45]. In a realistic simulation, we need to truncate the summation dimension up to a definite value n_d; namely, up to a phase factor $\exp[-i(l\omega_M + \Delta_k)t]$,

$$B_{n_0,l,k}^{n_d}(\infty) = \sum_{n=0}^{n_d-1} \frac{\sqrt{\frac{\gamma_c}{2\pi}}\,_b\langle l|\tilde{n}\rangle_b\,_b\langle\tilde{n}|n_0\rangle_b}{\left[\Delta_k + \delta - (n-l)\omega_M + i\frac{\gamma_c}{2}\right]}, \quad \text{(A1)}$$

where we add the superscript n_d to mark the summation dimension n_d.

To describe these Franck–Condon factors $_b\langle l|\tilde{n}\rangle_b$ and $_b\langle\tilde{n}|n_0\rangle_b$, we introduce a function

$$\begin{aligned}\mathcal{F}[m,n,\beta] &= {}_b\langle m|D_b(\beta)|n\rangle_b \\ &= \sqrt{\frac{(\min[m,n])!}{(\max[m,n])!}}e^{-\beta^2/2} \\ &\quad \times (\text{sgn}[m-n-1/2]\beta)^{\text{abs}[m-n]} \\ &\quad \times \text{LaguerreL}[\min[m,n],\text{abs}[m-n],\beta^2], \quad \text{(A2)}\end{aligned}$$

where $\max[x,y]$ and $\min[x,y]$ give the larger and smaller one between x and y, respectively; $\text{sgn}[x]$ gives -1, 0, or 1 depending on whether x is negative, zero, or positive, respectively; $\text{abs}[x]$ gives the absolute value of x, $\text{LaguerreL}[n,a,x]$ gives the generalized Laguerre polynomial $L_n^a(x)$. In terms of Eq. (A2), we can express these Franck–Condon factors as

$$_b\langle l|\tilde{n}\rangle_b = {}_b\langle l|D_b(\beta_0)|n\rangle_b = \mathcal{F}[l,n,\beta_0], \quad \text{(A3a)}$$
$$_b\langle\tilde{n}|n_0\rangle_b = {}_b\langle n|D_b^{\dagger}(\beta_0)|n_0\rangle_b = \mathcal{F}[n,n_0,-\beta_0]. \quad \text{(A3b)}$$

With the emission solution, we can reconstruct the density matrix of the mechanical mode.

2. Diagonal-density-matrix case

In the diagonal-density-matrix case, we consider the thermal state $\rho_{\text{th}}^{(b)} = \sum_{n=0}^{\infty} P_n|n\rangle\langle n|$, with $P_n = \bar{n}_{\text{th}}^n/(\bar{n}_{\text{th}}+1)^{n+1}$. The matrix $\mathbf{K}$ and the vector $\mathbf{Q}$ can be determined by

$$\mathbf{K}_{j,j'} = \sum_{l=0}^{n_{d_1}-1} \left|B_{j'-1,l,k_j}^{n_{d_1}}(\infty)\right|^2, \quad \text{(A4a)}$$

$$\mathbf{Q}_j = \sum_{n,l=0}^{n_{d_2}-1} \frac{\bar{n}_{\text{th}}^n}{(\bar{n}_{\text{th}}+1)^{n+1}}\left|B_{n,l,k_j}^{n_{d_2}}(\infty)\right|^2, \quad \text{(A4b)}$$

for $j,j' = 1,2,\ldots,N$. The vector $\mathbf{Q}$ is determined by experiments. Hence, in a realistic simulation, we need to choose a very large summation dimension n_{d_2}, which should be larger than the summation dimension n_{d_1} used in obtaining the matrix $\mathbf{K}$. Once we know the three system parameters g_0, γ_c, and ω_M, so the matrix $\mathbf{K}$ can be obtained.

We randomly generate a group of sample points in the region $\Delta_{k_j}/\omega_M \in [-5,5]$ (eight sample points, the truncation dimension $N = 8$). The locations of these points are

$$\Delta_{k_j}/\omega_M = [-0.238\,903, -4.152\,71, -2.181\,12, 4.7646, -4.457\,49, -3.345\,87, 4.921\,28, -0.3611\,81]. \quad \text{(A5)}$$

Using the parameters $n_{d_1} = 48$, $n_{d_2} = 60$, $g_0/\omega_M = 2$, $\gamma_c/\omega_M = 0.1$, and $\bar{n}_{\text{th}} = 1$, we numerically obtain the matrix

$$\mathbf{K} \approx \frac{10^{-2}}{\omega_M}\begin{pmatrix} 1.47341 & 1.00608 & 1.11404 & 0.68844 & 1.09823 & 0.88438 & 0.68566 & 0.85648 \\ 3.65773 & 4.03497 & 2.57462 & 2.59686 & 1.30956 & 2.41597 & 3.19158 & 2.85843 \\ 3.41250 & 1.63790 & 1.47325 & 1.71805 & 1.63361 & 1.60156 & 1.29623 & 1.45646 \\ 0.06990 & 0.07098 & 0.40837 & 1.06732 & 1.02115 & 0.63968 & 0.65275 & 0.74980 \\ 0.89358 & 0.83841 & 0.42001 & 0.63426 & 0.46637 & 0.64601 & 0.76208 & 0.63524 \\ 1.26672 & 0.81926 & 0.54281 & 0.61829 & 0.87052 & 0.58272 & 0.45410 & 0.68421 \\ 0.09186 & 0.85753 & 3.79587 & 6.18143 & 4.41536 & 3.26403 & 4.17912 & 4.42602 \\ 0.71383 & 0.72236 & 0.57617 & 0.36789 & 0.74751 & 0.44229 & 0.36831 & 0.56118 \end{pmatrix}, \quad \text{(A6)}$$

and the vector

$$\mathbf{Q} \approx \frac{10^{-2}}{\omega_M}(1.230\,94, 3.445\,40, 2.505\,07, 0.222\,98, 0.783\,67, 0.990\,37, 1.374\,27, 0.669\,94)^T. \tag{A7}$$

By numerically solving the equation $\mathbf{KP} = \mathbf{Q}$, we obtain the solution

$$\mathbf{P} \approx (0.501\,06, 0.249\,44, 0.125\,06, 0.063\,58, 0.031\,05, 0.015\,92, 0.005\,66, 0.007\,66)^T, \tag{A8}$$

which has a fidelity $F = 0.995$ with the exact phonon-number distribution

$$\mathbf{P}_{\text{exact}} = (0.5, 0.25, 0.125, 0.0625, 0.031\,25, 0.015\,625, 0.007\,812\,5, 0.003\,906\,25)^T. \tag{A9}$$

3. General density-matrix case

In the general density-matrix case, the elements of $\mathbf{M}$ are defined by

$$\mathbf{M}_{j,j'} = \sum_{l=0}^{n_{d_1}-1} \left[B_{n,l,k_j}^{n_{d_1}}(\infty)\right]^* B_{m,l,k_j}^{n_{d_1}}(\infty), \tag{A10}$$

for $j, j' \in [1,2,\ldots,N^2]$, where $m = \text{Floor}[(j'-1)/N]$ and $n = (j'-1) - mN$. The elements of the vector $\mathbf{S}$ are defined by

$$\mathbf{S}_j = \sum_{m,n,l=0}^{n_{d_2}-1} \rho_{m,n}^{(b)}(0)\left[B_{n,l,k_j}^{n_{d_2}}(\infty)\right]^* B_{m,l,k_j}^{n_{d_2}}(\infty), \tag{A11}$$

for $j \in [1,2,\ldots,N^2]$. In Eqs. (A10) and (A11), the probability amplitudes $B_{m(n),l,k_j}^{n_{d_{1(2)}}}(\infty)$ have been given in Eq. (A1).

As an example, we assume that the initial state of the mirror is $(|0\rangle_b + i|1\rangle_b - |2\rangle_b)/\sqrt{3}$, which has the density matrix

$$\rho_{\text{exact}}^{(b)}(0) = \frac{1}{3}\begin{pmatrix} 1 & -i & -1 \\ i & 1 & -i \\ -1 & i & 1 \end{pmatrix}. \tag{A12}$$

We choose a group of sample points which are located at the phonon-sideband peaks, with the locations $\Delta_{k_j} = -\delta + n\omega_M$ for $n \in [-4,4]$. Here we use the truncation dimension $N = 3$, and then choose nine sample points. Using the parameters $n_{d_1} = 48$, $n_{d_2} = 60$, $g_0/\omega_M = 2$, and $\gamma_c/\omega_M = 0.1$, then the locations of these sample points are

$$\Delta_{k_j}/\omega_M = [-8, -7, -6, -5, -4, -3, -2, -1, 0]. \tag{A13}$$

Based on Eqs. (A1), (A10), and (A11), we can numerically obtain the matrix

$$\mathbf{M} \approx \frac{10^{-1}}{\omega_M}$$

$$\times \begin{pmatrix}
2.65078 & 0.72701 + 0.06619i & 0.31389 + 0.04904i & \diamond & 2.73543 & 0.92622 + 0.09507i & \diamond & \diamond & 3.47639 \\
2.68039 & 0.78019 + 0.06690i & 0.50595 + 0.05111i & \diamond & 3.01083 & 1.1303 + 0.10038i & \diamond & \diamond & 2.86101 \\
2.79261 & 0.84290 + 0.06965i & 0.53053 + 0.05412i & \diamond & 3.12871 & 1.48178 + 0.10416i & \diamond & \diamond & 3.40431 \\
2.98886 & 1.00804 + 0.07440i & 0.57164 + 0.02008i & \diamond & 3.30036 & 1.37987 + 0.02789i & \diamond & \diamond & 3.50278 \\
3.26298 & 1.15702 + 0.05181i & 0.57538 - 0.10663i & \diamond & 3.49535 & 1.26968 - 0.08778i & \diamond & \diamond & 2.89283 \\
3.59519 & 1.17639 - 0.02772i & 0.24166 - 0.25788i & \diamond & 3.33098 & 0.76202 - 0.12633i & \diamond & \diamond & 2.43629 \\
3.86136 & 0.87698 - 0.13806i & -0.43399 - 0.29357i & \diamond & 2.78533 & -0.16378 - 0.10401i & \diamond & \diamond & 1.68726 \\
3.85851 & 0.08117 - 0.21613i & -1.30234 - 0.18395i & \diamond & 1.95965 & -0.72898 - 0.11875i & \diamond & \diamond & 1.76493 \\
3.38095 & -1.0129 - 0.22813i & -1.67703 - 0.02836i & \diamond & 1.51133 & -0.61621 - 0.17913i & \diamond & \diamond & 2.29425
\end{pmatrix}, \tag{A14}$$

and the vector

$$\mathbf{S} \approx \frac{10^{-1}}{\omega_M}(2.852\,46, 2.624\,96, 2.870\,73, 2.9511, 2.809\,48, 2.857\,02, 2.905\,94, 3.172\,67, 3.242\,02)^T. \tag{A15}$$

In the matrix $\mathbf{M}$, the elements denoted by "$\diamond$" can be determined by the following rule: In the same row, the elements with the column pairs $(2 \leftrightarrow 4)$, $(3 \leftrightarrow 7)$, and $(6 \leftrightarrow 8)$ are complex conjugate of each other. We can explain this property based on the relation $\Lambda_{n,m}(\Delta_{k_j}) = \Lambda_{m,n}^*(\Delta_{k_j})$ in Eq. (A10) and the following relations:

$$\mathbf{M}_{j,2} = \Lambda_{1,0}(\Delta_{k_j}), \quad \mathbf{M}_{j,4} = \Lambda_{0,1}(\Delta_{k_j}); \quad \mathbf{M}_{j,3} = \Lambda_{2,0}(\Delta_{k_j}), \quad \mathbf{M}_{j,7} = \Lambda_{0,2}(\Delta_{k_j}); \quad \mathbf{M}_{j,6} = \Lambda_{2,1}(\Delta_{k_j}), \quad \mathbf{M}_{j,8} = \Lambda_{1,2}(\Delta_{k_j}). \tag{A16}$$

In addition, the elements in the first, fifth, and ninth columns are real. This is because $\mathbf{M}_{j,1} = \Lambda_{0,0}(\Delta_{k_j})$, $\mathbf{M}_{j,5} = \Lambda_{1,1}(\Delta_{k_j})$, $\mathbf{M}_{j,9} = \Lambda_{2,2}(\Delta_{k_j})$, and $\Lambda_{n,n}(\Delta_{k_j})$ is real.

By numerically solving the equation $\mathbf{MC} = \mathbf{S}$, we obtain the expression of $\mathbf{C}$, which can be expressed in the density-matrix form as

$$\rho^{(b)}(0) \approx 0.333333 \begin{pmatrix} 1 & -i & -1 \\ i & 1 & -i \\ -1 & i & 1 \end{pmatrix}, \tag{A17}$$

where $\rho^{(b)}_{m,n}(0) = \mathbf{C}_l$. The relationship between m,n and l is $m = \text{Floor}[(l-1)/N]$ and $n = (l-1) - mN$, where $l = 1,2,3,\ldots,9$, and $m,n = 0,1,2$. The fidelity between the two density matrices $\rho^{(b)}_{\text{exact}}(0)$ and $\rho^{(b)}(0)$ is almost unity.

---

[1] U. Fano, Rev. Mod. Phys. **29**, 74 (1957).

[2] K. Vogel and H. Risken, Phys. Rev. A **40**, 2847(R) (1989).

[3] U. Leonhardt, *Measuring the Quantum State of Light* (Cambridge University Press, Cambridge, 1997).

[4] For reviews, see, e.g., A. I. Lvovsky and M. G. Raymer, Rev. Mod. Phys. **81**, 299 (2009); D.-G. Welsch, W. Vogel, and T. Opatrny, in *Progress in Optics*, edited by E. Wolf (Elsevier, Amsterdam, 1999), Vol. 39, p. 63.

[5] I. L. Chuang, L. M. K. Vandersypen, X. Zhou, D. W. Leung, and S. Lloyd, Nature (London) **393**, 143 (1998).

[6] A. G. White, D. F. V. James, P. H. Eberhard, and P. G. Kwiat, Phys. Rev. Lett. **83**, 3103 (1999).

[7] M. Steffen, M. Ansmann, R. C. Bialczak, N. Katz, E. Lucero, R. McDermott, M. Neeley, E. M. Weig, A. N. Cleland, and J. M. Martinis, Science **313**, 1423 (2006).

[8] D. T. Smithey, M. Beck, M. G. Raymer, and A. Faridani, Phys. Rev. Lett. **70**, 1244 (1993).

[9] S. Schiller, G. Breitenbach, S. F. Pereira, T. Müller, and J. Mlynek, Phys. Rev. Lett. **77**, 2933 (1996).

[10] G. Breitenbach, S. Schiller, and J. Mlynek, Nature (London) **387**, 471 (1997).

[11] A. I. Lvovsky, H. Hansen, T. Aichele, O. Benson, J. Mlynek, and S. Schiller, Phys. Rev. Lett. **87**, 050402 (2001).

[12] A. Ourjoumtsev, R. Tualle-Brouri, and P. Grangier, Phys. Rev. Lett. **96**, 213601 (2006).

[13] S. Deléglise, I. Dotsenko, C. Sayrin, J. Bernu, M. Brune, J.-M. Raimond, and S. Haroche, Nature (London) **455**, 510 (2008).

[14] M. Brune, J. Bernu, C. Guerlin, S. Deléglise, C. Sayrin, S. Gleyzes, S. Kuhr, I. Dotsenko, J. M. Raimond, and S. Haroche, Phys. Rev. Lett. **101**, 240402 (2008).

[15] M. Hofheinz, H. Wang, M. Ansmann, R. C. Bialczak, E. Lucero, M. Neeley, A. D. O'Connell, D. Sank, J. Wenner, J. M. Martinis, and A. N. Cleland, Nature (London) **459**, 546 (2009).

[16] H. Wang, M. Hofheinz, M. Ansmann, R. C. Bialczak, E. Lucero, M. Neeley, A. D. O'Connell, D. Sank, M. Weides, J. Wenner, A. N. Cleland, and J. M. Martinis, Phys. Rev. Lett. **103**, 200404 (2009).

[17] F. Mallet, M. A. Castellanos-Beltran, H. S. Ku, S. Glancy, E. Knill, K. D. Irwin, G. C. Hilton, L. R. Vale, and K. W. Lehnert, Phys. Rev. Lett. **106**, 220502 (2011).

[18] C. Eichler, D. Bozyigit, C. Lang, L. Steffen, J. Fink, and A. Wallraff, Phys. Rev. Lett. **106**, 220503 (2011).

[19] Y. Shalibo, R. Resh, O. Fogel, D. Shwa, R. Bialczak, J. M. Martinis, and N. Katz, Phys. Rev. Lett. **110**, 100404 (2013).

[20] D. Leibfried, D. M. Meekhof, B. E. King, C. Monroe, W. M. Itano, and D. J. Wineland, Phys. Rev. Lett. **77**, 4281 (1996).

[21] C. Kurtsiefer, T. Pfau, and J. Mlynek, Nature (London) **386**, 150 (1997).

[22] L. G. Lutterbach and L. Davidovich, Phys. Rev. Lett. **78**, 2547 (1997).

[23] T. J. Dunn, I. A. Walmsley, and S. Mukamel, Phys. Rev. Lett. **74**, 884 (1995).

[24] L. J. Waxer, I. A. Walmsley, and W. Vogel, Phys. Rev. A **56**, R2491(R) (1997).

[25] P. Rabl, A. Shnirman, and P. Zoller, Phys. Rev. B **70**, 205304 (2004).

[26] S. Singh and P. Meystre, Phys. Rev. A **81**, 041804 (2010).

[27] H. Miao, S. Danilishin, H. Müller-Ebhardt, H. Rehbein, K. Somiya, and Y. Chen, Phys. Rev. A **81**, 012114 (2010).

[28] M. R. Vanner, I. Pikovski, G. D. Cole, M. S. Kim, Č. Brukner, K. Hammerer, G. J. Milburn, and M. Aspelmeyer, Proc. Natl. Acad. Sci. USA **108**, 16182 (2011).

[29] M. R. Vanner, J. Hofer, G. D. Cole, and M. Aspelmeyer, Nat. Commun. **4**, 2295 (2013).

[30] T. J. Kippenberg and K. J. Vahala, Science **321**, 1172 (2008).

[31] M. Aspelmeyer, T. J. Kippenberg, and F. Marquardt, arXiv:1303.0733.

[32] I. Wilson-Rae, N. Nooshi, W. Zwerger, and T. J. Kippenberg, Phys. Rev. Lett. **99**, 093901 (2007).

[33] F. Marquardt, J. P. Chen, A. A. Clerk, and S. M. Girvin, Phys. Rev. Lett. **99**, 093902 (2007).

[34] J. D. Teufel, T. Donner, D. Li, J. W. Harlow, M. S. Allman, K. Cicak, A. J. Sirois, J. D. Whittaker, K. W. Lehnert, and R. W. Simmonds, Nature (London) **475**, 359 (2011).

[35] J. Chan, T. P. Mayer Alegre, A. H. Safavi-Naeini, J. T. Hill, A. Krause, S. Gröblacher, M. Aspelmeyer, and O. Painter, Nature (London) **478**, 89 (2011).

[36] D. Vitali, S. Gigan, A. Ferreira, H. R. Böhm, P. Tombesi, A. Guerreiro, V. Vedral, A. Zeilinger, and M. Aspelmeyer, Phys. Rev. Lett. **98**, 030405 (2007).

[37] Y. D. Wang and A. A. Clerk, Phys. Rev. Lett. **110**, 253601 (2013).

[38] L. Tian, Phys. Rev. Lett. **110**, 233602 (2013).

[39] A. Mari and J. Eisert, Phys. Rev. Lett. **103**, 213603 (2009).

[40] J. Q. Liao and C. K. Law, Phys. Rev. A **83**, 033820 (2011).

[41] G. F. Xu and C. K. Law, Phys. Rev. A **87**, 053849 (2013).

[42] X. W. Xu, H. Wang, J. Zhang, and Y. X. Liu, Phys. Rev. A **88**, 063819 (2013).

[43] L. F. Buchmann, H. Jing, C. Raman, and P. Meystre, Phys. Rev. A **87**, 031601(R) (2013).

[44] O. Romero-Isart, A. C. Pflanzer, M. L. Juan, R. Quidant, N. Kiesel, M. Aspelmeyer, and J. I. Cirac, Phys. Rev. A **83**, 013803 (2011).

[45] J. Q. Liao, H. K. Cheung, and C. K. Law, Phys. Rev. A **85**, 025803 (2012).

[46] J. Q. Liao and C. K. Law, Phys. Rev. A **87**, 043809 (2013).

[47] C. K. Law, Phys. Rev. A **51**, 2537 (1995).

[48] X. Hu and F. Nori, Phys. Rev. Lett. **76**, 2294 (1996); **79**, 4605 (1997).

[49] M. Ludwig, B. Kubala, and F. Marquardt, New J. Phys. **10**, 095013 (2008).

[50] K. W. Murch, K. L. Moore, S. Gupta, and D. M. Stamper-Kurn, Nat. Phys. **4**, 561 (2008).

[51] P. Rabl, Phys. Rev. Lett. **107**, 063601 (2011).

[52] A. Nunnenkamp, K. Børkje, and S. M. Girvin, Phys. Rev. Lett. **107**, 063602 (2011).

[53] T. T. Heikkilä, F. Massel, J. Tuorila, R. Khan, and M. A. Sillanpää, Phys. Rev. Lett. **112**, 203603 (2014).

[54] A. J. Rimberg, M. P. Blencowe, A. D. Armour, and P. D. Nation, New J. Phys. **16**, 055008 (2014).

[55] J. Q. Liao, K. Jacobs, F. Nori, and R. W. Simmonds, New J. Phys. **16**, 072001 (2014).

[56] X.-Y. Lü, W.-M. Zhang, S. Ashhab, Y. Wu, and F. Nori, Sci. Rep. **3**, 2943 (2013).

[57] A. Xuereb, C. Genes, and A. Dantan, Phys. Rev. Lett. **109**, 223601 (2012); Phys. Rev. A **88**, 053803 (2013).

[58] R. H. Hadfield, Nat. Photonics **3**, 696 (2009).

[59] J. D. Thompson, B. M. Zwickl, A. M. Jayich, F. Marquardt, S. M. Girvin, and J. G. E. Harris, Nature (London) **452**, 06715 (2008).

[60] J. M. Raimond, M. Brune, and S. Haroche, Rev. Mod. Phys. **73**, 565 (2001).